Mitigation of Plasma Effects in High Pressure RF Cavity for Ionization Cooling

Moses Chung, Alvin Tollestrup, Andreas Jansson, Katsuya Yonehara, and David Neuffer
Accelerator Physics Center, Fermi National Accelerator Laboratory, Batavia, IL 60510
(Dated: January 30, 2009)

In this note, we summarize the possible effects of plasma formation during beam propagation through the gas-filled pressurized RF cavity. To mitigate detrimental effects, use of a dopant gas with high electron attachment rate has been discussed.

I. INTRODUCTION

Ionization cooling is the critical building block for the realization of a neutrino factory and a muon collider, because only this cooling scheme can reduce the emittance of the intense muon beam fast enough compared to the short muon lifetime [1–3]. Recently, the idea of using high-pressure hydrogen gas as an energy absorber has been proposed [4]. In particular, when RF cavities are pressurized, there are two unique advantages. First, the momentum loss (both in the transverse and longitudinal directions) and the momentum regain (only in the longitudinal direction) happen simultaneously rather than sequentially. Second, higher accelerating field gradient and better breakdown suppression are possible due to the Paschen effect.

Initial experiments of High-Pressure RF (HPRF) cavity in the absence of the beam have demonstrated that higher field gradients are possible compared to the case of the conventional evacuated cavities [4]. When an intense beam is present, however, several factors associated with the plasma formation may limit the performance of the HPRF cavity [5]. To demonstrate the feasibility of using HPRF cavities in the actual cooling channel, a beam test is planned in the MuCool Test Area (MTA) of Fermilab in early 2009. Since an intense muon beam is not available, a proposed beam test will use proton beam injected from the linac.

In this note, we will discuss several physics issues associated with the formation of the plasma column induced by the beam and possible mitigation methods for them.

II. IONIZATION COOLING

The equation describing the rate of change of the normalized transverse emittance ϵ_n within the absorber is given by the balance between the energy-loss cooling (first term) and the multiple-scattering heating (second term) effects [1–3]:

$$\frac{d\epsilon_n}{ds} = -\frac{1}{\beta^2}\frac{1}{E}\frac{dE}{ds}\epsilon_n + \frac{\beta\gamma}{2\beta^4}\frac{E_s^2}{E^2}\frac{\beta_\perp}{L_R}. \tag{1}$$

Here, $E = \gamma m_b c^2$ is the beam particle energy, E_s is the characteristic scattering energy, $dE/ds = \rho dE/dx$ is the mean rate of energy loss (or stopping power), L_R is the radiation length of the absorber medium, $\beta_\perp (= \beta_x = \beta_y)$ is the transverse beta-function of the magnetic channel, and $\beta = v/c$ and $\gamma = (1-\beta^2)^{-1/2}$ are the usual relativistic factors. The normalized emittance ϵ_n is related to the geometric rms emittance $\epsilon_\perp (= \epsilon_x = \epsilon_y)$ by $\epsilon_n = \epsilon_\perp(\beta\gamma)$ and the transverse beam size is given by $\sqrt{\langle x^2\rangle} = \sqrt{\langle y^2\rangle} = (\epsilon_\perp \beta_\perp)^{1/2}$.

A. Energy-loss cooling

The energy lost by a beam particle with atomic number z as it propagates through a medium is given by the Bethe-Bloch equation [6],

$$\frac{dE}{ds} = Kz^2\frac{Z}{A}\frac{\rho}{\beta^2}\left[\frac{1}{2}\ln\left(\frac{2m_e c^2\beta^2\gamma^2 T_{\max}}{I^2}\right) - \beta^2 - \frac{\delta}{2}\right]. \tag{2}$$

Here, $K = 0.3071$ MeV g^{-1}cm^2, Z/A is the ratio of atomic number to weight, ρ is the mass density of the medium in g/cm^3, I is the mean excitation energy in eV. $T_{\max}$ is the maximum kinetic energy which can be transferred to a free electron in a single collision, which is approximated as $T_{\max} \approx 2m_e c^2\beta^2\gamma^2$ in the low-energy approximation, and δ is the density effect correction which is small at low energy. For the beam test of a HPRF cavity experiment, the kinetic energy of the proton beam inside the cavity is estimated to be $T \approx 200$ MeV [7], which yields the stopping power of $dE/dx \approx 10$ MeV cm^2/g in the molecular hydrogen (see Fig. 1). Note that when $\partial(dE/dx)/\partial T < 0$, lower energy particle loses more energy than higher energy particles, increasing the longitudinal energy spread.

B. Multiple-scattering heating

The rms scattering angle can be given in terms of the radiation length L_R [8]:

$$\theta_{\rm rms} = \sqrt{\langle\theta^2\rangle} \simeq \frac{1}{\beta^2}\frac{E_s}{E}\sqrt{\frac{\Delta s}{L_R}}, \tag{3}$$

where Δs is the thickness of material. In the limit of small angle, $\frac{1}{2}\theta_{\rm rms}^2 = \langle\theta_x^2\rangle \simeq \Delta\langle x'^2\rangle$, where the factor $\frac{1}{2}$ comes from the projection of the deflection angle into the $x-s$ plane. The radiation length L_R is a function of scattering material given by

$$L_R = \frac{X_0}{\rho} = \frac{716.4\times A}{Z(Z+1)\ln(287/\sqrt{Z})}\frac{1}{\rho}. \tag{4}$$

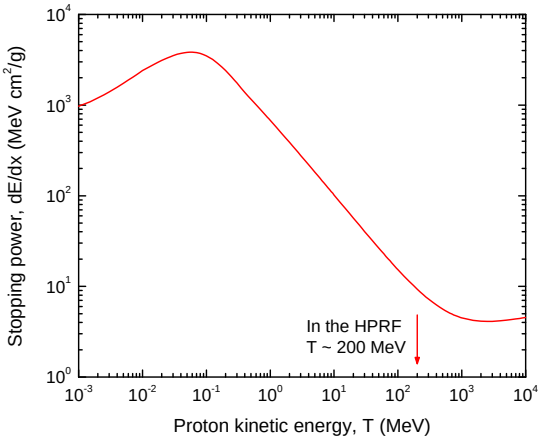

FIG. 1: Stopping power for protons in molecular hydrogen [6]. During passing through the thick (∼5 cm) cavity wall, electrons are stripped off from the initial H^- beam and resultant proton beam slows down from $T \sim 400$ to 200 MeV, which is slightly lower than minimum ionization.

Since, the rms emittance is $\epsilon_\perp = \sqrt{\langle x^2\rangle \langle x'^2\rangle} = \langle x'^2\rangle \beta_\perp$ at a beam waist, the increase in the rms emittance during the transit of Δs around the beam waist is approximated as

$$\Delta\epsilon_\perp \simeq \beta_\perp \Delta \langle x'^2\rangle \simeq \frac{\beta_\perp}{2}\theta_{\rm rms}^2. \tag{5}$$

Hence, we have

$$\frac{\Delta\epsilon_\perp}{\Delta s} \simeq \frac{\beta_\perp}{2}\frac{\theta_{\rm rms}^2}{\Delta s} \simeq \frac{\beta_\perp}{2}\frac{1}{\beta^4}\frac{E_s^2}{E^2}\frac{1}{L_R}, \tag{6}$$

which corresponds to the second term of the Eq. (1). Note that emittance increase from multiple-scattering depends on beam size.

III. PLASMA FORMATION

A. Beam-impact ionization

During propagation through a gas, the incident beam undergoes ionizing collisions with neutral gas molecules (as intended for ionization cooling). For the ionization of hydrogen molecules by fast proton impact, single-ionization is dominant [10].

$$\mathrm{p} + \mathrm{H_2} \longrightarrow \mathrm{p} + \mathrm{H_2^+} + \mathrm{e^-} \tag{7}$$

Most of the energy lost by protons through collisions goes into ionization, which leads to the build up of an electron/ion plasma in the volume of the beam path.

The electrons ejected from the primary ionization can have enough energy (larger than the ionization potential E_i of the gas) to further ionize, producing secondary electron/ion pairs through following processes:

$$\mathrm{e^-} + \mathrm{H_2} \longrightarrow \mathrm{H_2^+} + 2\mathrm{e^-} \tag{8}$$

$$\mathrm{e^-} + \mathrm{H_2} \longrightarrow \mathrm{H} + \mathrm{H^+} + 2\mathrm{e^-} \tag{9}$$

Normally, the dissociative ionization (9) is much smaller than the ionization (8) [11], and $n_e \approx n_{\mathrm{H_2^+}}$ to good approximation. The total electron line density after one micropulse ($\sim 10^9$ protons) of the beam passes through the cavity is conveniently expressed by

$$N_L = n_e \pi r_b^2 = \frac{\rho dE/dx}{W_i} \times 10^9, \tag{10}$$

where $r_b = \sqrt{2\langle x^2 + y^2\rangle}$ is the radius of a uniform-density beam, and W_i is the effective average energy to produce an electron/ion pair. Because some energy loss goes to just molecule excitation, the W_i-value is typically about twice larger than the ionization potential E_i. The mass density of the hydrogen gas can be expressed in terms of the pressure as $\rho[\mathrm{g/cm^3}] = 5.6 \times 10^{-6} p[\mathrm{psi}]$ for $T_{\rm room} = 300$ K.

For the analysis of electron evolution at the macropulse time scale, we define the average electron source term as

$$S\left[\mathrm{cm^{-3}s^{-1}}\right] \approx \frac{N_L/\pi r_b^2}{\Delta t_p}. \tag{11}$$

Note that, in fact, micropulse duration ($\sim$ 0.13 ns) is much shorter than the micropulse spacing ($\Delta t_p = 5$ ns).

B. Production of energetic electrons (δ rays)

During beam-impact ionization, the ejected electron can have a kinetic energy up to the maximum allowed $T_{\rm max}$. The distribution of electrons with kinetic energy T is approximately given by [12]

$$\frac{dN}{dT} \approx \frac{1}{2} K z^2 \frac{Z}{A}\frac{\rho\Delta s}{\beta^2}\frac{1}{T^2}. \tag{12}$$

Integration of Eq. (12) yields an expression for the number of electrons ejected at a kinetic energy larger than or equal to T_0 as [12]

$$N(T \geq T_0) \approx \frac{1}{2} K z^2 \frac{Z}{A}\frac{\rho\Delta s}{\beta^2}\left[\frac{1}{T_0} - \frac{1}{T_{\rm max}}\right]. \tag{13}$$

Before completely slowing down through elastic and inelastic collisions with background gas molecules, energetic electrons will cover a certain distance in the gas. An approximate expression for the practical range (the effective distance including the randomizing effect of the multiple collisions) as a function of electron kinetic energy up to a few hundred keV is [12]

$$R_p[\mathrm{cm}] \approx \frac{0.5}{Z/A} \times 0.71 \times (T[\mathrm{MeV}])^{1.72}/\rho. \tag{14}$$

Material	Z	A	$< Z/A >$	I [eV]	W_i [eV]	E_i [eV]	X_0 [g cm^{-2}]
H_2	1	1.00794	0.99212	19.2	37	15.42	63.04

TABLE I: Atomic properties of molecular hydrogen [6, 9] used in this note.

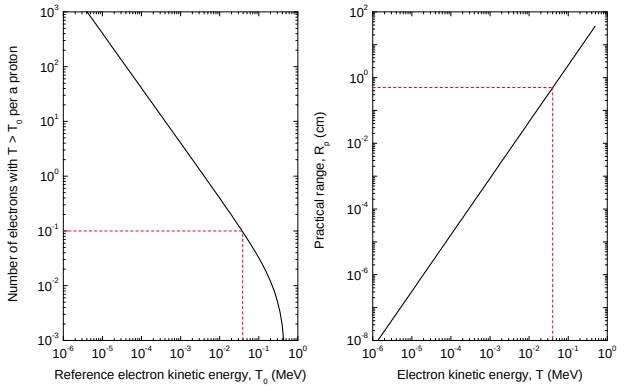

FIG. 2: Number of energetic electrons ejected with $T \geq T_0$ (left) and practical range of electrons (right) in molecular hydrogen. Here, we set $p = 500$ psi and $\Delta s = 3$ cm.

When $R_p \sim 1$ cm, we expect energetic electrons to hit the cavity wall and have some noticeable effects (for example, secondary electron emission). Nonetheless, from Fig. 2, we note that only one out of ten protons ejects a 40 keV electron that has $R_p \sim 1$ cm.

C. Electron thermalization

For the nominal operating conditions of the HPRF cavity ($f = \omega/2\pi \approx 805$ MHz), ions can be assumed to be immobile. On the other hand, electrons not only interact with the external RF field, but also suffer collisions with background gas molecules. The total electron-neutral collision frequency for momentum transfer is approximately given $\nu_m \approx 4.4 \times 10^9 p[\text{torr}] \approx 2.3 \times 10^{11} p[\text{psi}]$ for $4 < E/p < 30$ and $T_{\text{room}} = 300$ K [13, 14], and the response of plasma electrons to the external RF field is described by conductivity:

$$\sigma = \frac{n_e e^2}{m_e \nu_m} \left[\frac{\nu_m^2}{\nu_m^2 + \omega^2} - i \frac{\omega \nu_m}{\nu_m^2 + \omega^2} \right]. \tag{15}$$

A typical axial drift motion of an electron in the RF field in the limit of very high frequency collisions is illustrated in Fig. 3, together with the micropulse duration and spacing. The maximum axial displacement is $z_0 \approx eE_0/(m_e \nu_m \omega)$.

The real component of the plasma conductivity (15) leads to the resistive heating of electrons, and the average power transferred from RF field through collisions can be

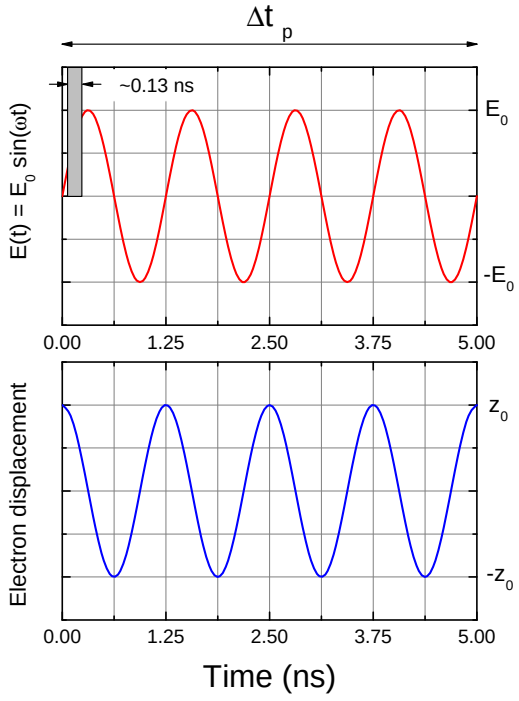

FIG. 3: Illustrative example of axial drift motion of an electron in RF field in the limit of very high frequent collisions. The displacement is shifted in phase ($\approx \pi/2$) relative to the field.

written as

$$P_c = \frac{n_e e^2 E_{\text{rms}}^2}{m_e(\nu_m^2 + \omega^2)} \nu_m, \tag{16}$$

where $E_{\text{rms}}^2 = E_0^2/2$ is the rms electric field. The balance of electron thermal energy ϵ is made up of gaining energy from the field and transferring it to the gas molecules (elastic or inelastic):

$$\frac{d\epsilon}{dt} = \left[\frac{P_c}{n_e \nu_m} - \delta_\epsilon \epsilon \right] \nu_m, \tag{17}$$

where δ_ϵ is the fractional energy loss. During slowing down in the energy range below the ionization potential, electrons mostly dissipate energy by exciting the vibrational and rotational energy levels of molecular hydrogen. In this case, $\delta_\epsilon \approx (2m_e/m_{\text{H}_2}) \sim 10 \times (2m_e/m_{\text{H}_2})$ [15]. The time required for the electrons to reach a new equilibrium is approximately given by $\tau_\epsilon \approx 1/\delta_\epsilon \nu_m$, and the final equilibrium energy is approximated for $\nu_m \gg \omega$

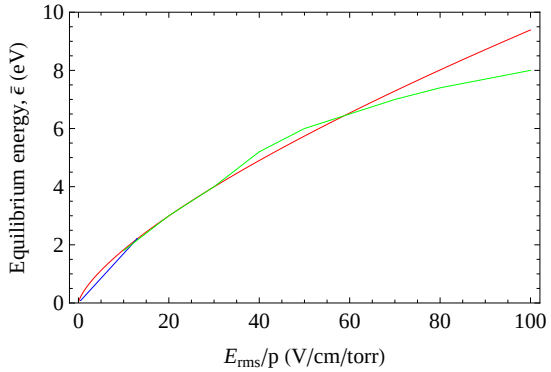

FIG. 4: Equilibrium energy of electrons in the hydrogen molecules as a function of $E_{\rm rms}/p$ estimated by Heylen [16] (red), Brown [17] (green), and Raizer [14] (blue).

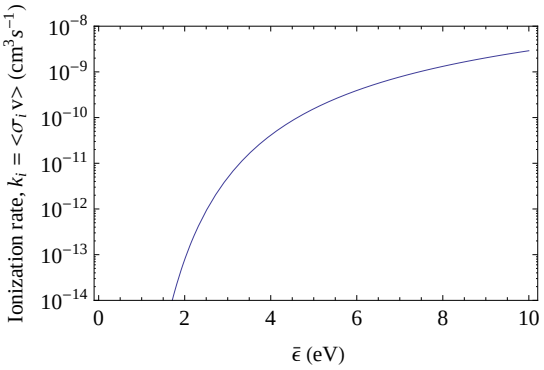

FIG. 5: Ionization rate coefficient as a function of average electron energy.

as

$$\bar{\epsilon} = \frac{1}{2} m_e \left\langle v_x^2 + v_y^2 + v_z^2 \right\rangle = \frac{3}{2} T_e \approx \frac{e^2 E_{\rm rms}^2}{m_e \nu_m^2 \delta_\epsilon}. \qquad (18)$$

If δ_ϵ and ν_m are independent of energy, we obtain $\bar{\epsilon} \propto (E_{\rm rms}/p)^2$. More accurately, the equilibrium energy is determined from experiments as a function of a combined parameter, $E_{\rm rms}/p$ (see Fig. 4). When RF is off ($E_{\rm rms} \to 0$), electrons are thermalized and acquire the gas temperature $T_{\rm room}$ within a short time period τ_ϵ.

IV. POSSIBLE PLASMA EFFECTS

A. Breakdown

Breakdown is a threshold process, which is a consequence of the steep dependence of the ionization rate on $E_{\rm rms}/p$ (see Figs. 4 and 5). In equilibrium, molecules are ionized by high-energy electrons in the tail of the Maxwellian distribution, and the ionization rate is given by [14]

$$k_i = \langle \sigma_i v \rangle = C_i \left(\frac{8T_e}{\pi m_e} \right)^{1/2} (E_i + 2T_e) \exp\left(-\frac{E_i}{T_e} \right), \qquad (19)$$

where $C_i = 0.59 \times 10^{-17} \mathrm{cm}^2/\mathrm{eV}$ for a hydrogen molecule. When the ionization rate exceeds the electron removal rate, an electron avalanche will develop and eventually shunt the RF cavity. A simplified rate equation for the electron density with possible electron removal processes can be written as

$$\frac{dn_e}{dt} = S + (k_i - k_{\rm DA}) n_{\rm H_2} n_e - \beta_r n_e^2 - \frac{D}{\Lambda^2} n_e, \qquad (20)$$

where S is a source term (from beam-impact ionization), $k_{\rm DA}$ is the rate coefficient for dissociative attachment (DA) to background hydrogen molecules, β_r is a recombination coefficient, and D and Λ are diffusion coefficient and length respectively.

At high pressure, diffusion is often negligible and recombination is slow compared to other processes. Only dissociative attachment,

$$\mathrm{e}^- + \mathrm{H}_2 \longrightarrow \mathrm{H} + \mathrm{H}^-, \qquad (21)$$

can be a possible mechanism for impeding breakdown in short time scale [14]. Hence, the condition for electron avalanche can be expressed as $k_i > k_{\rm DA}$ or in terms of a threshold value $(E_{\rm rms}/p)_{\rm t}$ as $E_{\rm rms}/p > (E_{\rm rms}/p)_{\rm t}$, where $k_i[(E_{\rm rms}/p)_{\rm t}] = k_{\rm DA}[(E_{\rm rms}/p)_{\rm t}]$. Note that even if $k_i < k_{\rm DA}$, there will be a linear increase of the electron density due to the source term. Since only the lowest vibrational level ($v = 0$) of the ground electronic state of H_2 is populated at room temperature ($T_{\rm room} = 300$ K), the rate of this process is typically less than $k_{\rm DA} \sim 10^{-14}$ cm^{3}s^{-1} [18, 19]. Hence, from Figs. 4 and 5, we expect that only if $E_{\rm rms}/p \geq 10$ V/cm/torr, then $\bar{\epsilon} \geq 2$ eV, $k_i \geq k_{\rm DA}$, and breakdown can be triggered.

On the other hand, the electron attachment rate is known to increase dramatically with increasing vibrational energy. For example, the rate coefficient approaches to the maximum value of $k_{\rm DA} \sim 10^{-8}$ cm^{3}s^{-1} for excited vibrational levels around $v = 9$ [18, 19]. Nonetheless, the average energy deposited from one proton micropulse to a hydrogen molecule is only $\Delta E \sim 10^9 \times (\rho dE/dx)/(n_{\rm H_2} \pi r_b^2) \sim 10^{-8}$ eV, and the heating effect of a hydrogen molecule by collisions with electrons during one RF cycle is only $\Delta E \sim (e^2 E_{\rm rms}^2/m_e \nu_m^2) \times (\nu_m/f) \times (n_e/n_{\rm H_2}) \sim 10^{-7}$ eV. Therefore, vibrational excitation ($\Delta E > 0.1$ eV) is expected to be limited for typical HPRF experiment conditions. To obtain dissociative attachment that is effective in removing electrons, one might consider exciting the higher vibrational states by an infrared laser irradiation [20].

B. Decrease in quality factor

In the absence of breakdown, dissociative recombination is the dominant mechanism for bulk removal of elec-

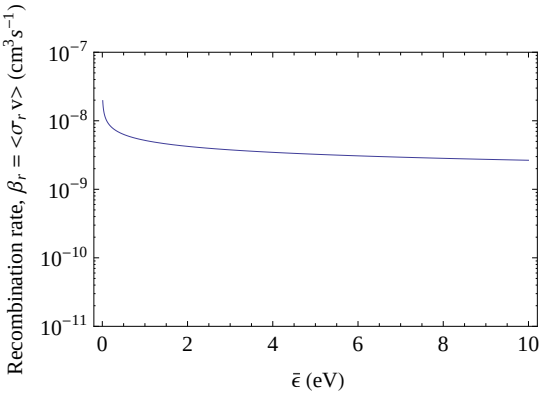

FIG. 6: Dissociative recombination rate coefficient as a function of average electron energy [21, 22].

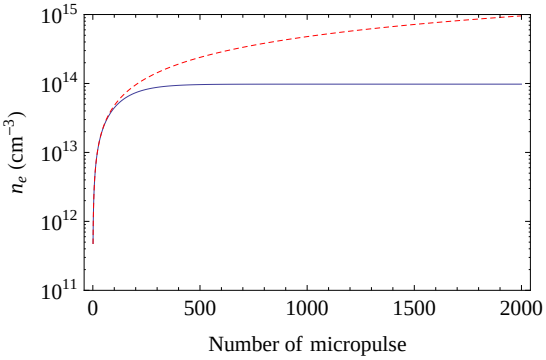

FIG. 7: Examples of electron density evolution over many micropulses without (red) and with (blue) recombination. Here, we pick the parameters to $\beta_r \sim 10^{-8}\mathrm{cm}^3\mathrm{s}^{-1}$, $r_b \sim 1$ cm, $p = 1000$ psi.

trons in a weakly ionized plasma where molecular ions are abundant [14].

$$\mathrm{e}^- + \mathrm{H}_2^+ \longrightarrow \mathrm{H(n=1)} + \mathrm{H}^*\mathrm{(n>1)} \tag{22}$$

Recombination does not greatly influence the breakdown threshold. The fate of an avalanche (whether it will grow or die out) is decided at its early stage, in which the number of electron/ion pairs is so small that recombination has a very low probability (note that the recombination rate is proportional to the electron density squared). On the other hand, recombination can finalize the electron density level reached by beam-impact ionization during the propagation of macropulse (many short micropulses) in the microsecond to millisecond range. The electron density evolution during the macropulse is determined by [23]

$$\frac{dn_e}{dt} = S - \beta_r n_e^2, \tag{23}$$

which results in

$$n_e = \sqrt{\frac{S}{\beta_r}} \left(\frac{1 - e^{-2\sqrt{S\beta_r}t}}{1 + e^{-2\sqrt{S\beta_r}t}} \right). \tag{24}$$

Note that for $\beta_r \to 0$, $n_e = St$ and for $t \to \infty$, $n_e = \sqrt{S/\beta_r}$. The recombination time scale is estimated to be $(S\beta_r)^{-1/2} \approx 1$ μsec for $\beta_r \sim 10^{-8}\mathrm{cm}^3\mathrm{s}^{-1}$ and $p = 1000$ psi.

Even though the plasma density is expected to be saturated somehow in the absence of breakdown, the locally accumulated plasma will eventually degrade the performance of the RF cavity. When the cavity is filled with a plasma of complex conductivity [Eq. (15)], the imaginary part causes the shift in the resonance frequency ω_0 and the real part the decrease in the Q value. They are given by Slater's perturbation equations [24]:

$$2\frac{\Delta\omega_0}{\omega_0} = \frac{1}{1 + (\nu_m/\omega_0)^2} \frac{\langle n_e \rangle}{n_c}, \tag{25}$$

$$\Delta\left(\frac{1}{Q}\right) = \frac{(\nu_m/\omega_0)}{1 + (\nu_m/\omega_0)^2} \frac{\langle n_e \rangle}{n_c}, \tag{26}$$

where

$$\langle n_e \rangle = \frac{\int_V n_e E_0^2(r,z) dV}{\int_V E_0^2(r,z) dV}, \tag{27}$$

and $n_c = \epsilon_0 m_e \omega_0^2 / e^2$ is the critical density. Here, we assume that the plasma is highly collisional ($\omega_{pe}^2 = n_e e^2/\epsilon_0 m_e \ll \nu_m^2$ and $\omega_0^2 \ll \nu_m^2$) that the electron current is small compared to the displacement current, and the electric field is altered only slightly from the initial spatial distribution $E_0(r,z)$. Equation (27) indicates that the effect accumulated electrons is large at places where E_0 is large. If the plasma consists of a small radius uniform column ($r \approx r_b$), much smaller than the cavity radius R_c, we can approximate

$$\langle n_e \rangle \approx n_e \times \frac{r_b^2}{\xi R_c^2}, \tag{28}$$

where the geometric factor ξ is calculated to be 0.2695 for the case of a simple pill box cavity. The plasma column may be looked upon as a lumped admittance, shunting the cavity. Since the change in the resonance frequency is of the order of $\sim (\omega_0/\nu_m)^2 \ll 1$, the dominant effect of this plasma column will be the decrease in the loaded Q, Q_L. Combining Eqs. (26) and (28), we can estimate the change in the Q_L of the cavity according to the propagation of the macropulse. As is apparent in Fig. 8, if the plasma is not removed properly, we expect a significant reduction in the quality factor within a few tens of micropulses.

In calculating Eq. (26), we have assumed that the collision frequency is linearly proportional to the pressure and independent of the applied RF electric field. This assumption is not valid for high collisional regime as discussed in Appendix A.

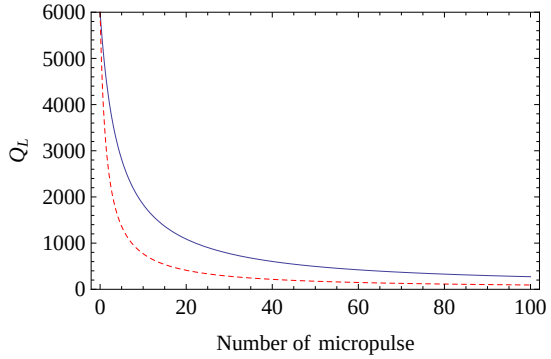

FIG. 8: Decreases in Q_L over many micropulses are plotted without (blue straight line) and with (red dotted line) correction for low values of E_0/p. Here, we assume $Q_L = 6000$ initially, $p = 1000$ psi, and $E_0/p \sim 1$ V/cm/torr.

C. Enhanced multiple scattering

When a beam ion collides with a background neutral gas, no force is felt until the beam ion is close to the gas molecule, on the scale of atomic dimensions. If the incident beam ion doesn't approach within atomic dimensions, then the nucleus of the gas molecule is shielded by its bound electrons [25]. When a plasma column is created along the beam path, however, scattering through the plasma column may extend the range of Coulomb interactions. In particular, there is a possibility that small-angle long-range Coulomb scattering between beam ions and background molecular ions could increase the deflection of the beam ion velocity vector [26]. Note that collisions between beam ions and plasma electrons will not contribute to the deflection due to the large mass ratio, $m_b/m_e \gg 1$. For $n_i \approx n_{H_2^+} \approx n_e$ and $m_i = 2m_b$, the scattering angle can be approximated as [26, 27]

$$\left\langle \theta_x^2 \right\rangle_i \approx \frac{n_i z^2 Z_i^2 e^4}{4\pi\epsilon_0^2 E^2 \beta^4} \ln\Lambda \times \Delta s. \tag{29}$$

Here, $\ln\Lambda$ is the Coulomb logarithm [25, 27]. By comparing Eqs. (3) and (29), we have the following ordering:

$$\frac{\left\langle \theta_x^2 \right\rangle_i}{\left\langle \theta_x^2 \right\rangle} \sim O\left(\frac{n_e}{n_{H_2}}\right) \ll 1. \tag{30}$$

Hence, the contribution of the plasma to the multiple scattering is negligible.

From Eqs. (4) and (29), we note that enhanced multiple scattering can be an issue when high-Z impurities are accumulated inside the cavity (for example, when too much dopant gas is applied).

V. MITIGATION OF PLASMA EFFECTS USING A DOPANT GAS

When plasma electrons are accumulated, the performance of the RF cavity will be degraded considerably. In order to remove plasma electrons, use of a dopant gas with high electron attachment cross section has been proposed. Here, we consider SF_6 (sulphur hexafluoride) and c-C_4F_8 (perfluorocyclobutane).

With a dopant gas, the average lifetime of a beam-induced electron is determined by the sum of the time needed for the electron to be thermalized to an energy level at which attachment becomes significant, $\tau_\epsilon \approx 1/(\delta_\epsilon \nu_m)$, plus the average time required before the electron is then captured, $\tau_a \approx 1/(k_a \alpha n_g)$ [23]. Here, k_a is the electron attachment rate coefficient (see Fig. 9), $\alpha = n_{\rm dop}/n_g = p_{\rm dop}/p$ is the partial fraction of dopant in the gas mixture, and $n_g[\mathrm{cm}^{-3}] = 1.7 \times 10^{18} p[\mathrm{psi}]$ for $T_{\rm room} = 300$ K. If $\tau_\epsilon + \tau_a < \Delta t_p$, then the equilibrium electron density is approximately given by

$$n_e \approx S(\tau_\epsilon + \tau_a). \tag{31}$$

When $\tau_\epsilon + \tau_a > \Delta t_p$, the dopant gas cannot fully remove the electrons before next micropulse comes. The minimum effective dopant fraction is, for example, $\alpha \approx 0.0006\%$ for $p = 1000$ psi. Once the dopant fraction is high enough that the attachment time is comparable to the energy equilibration time, little further benefit is obtained by increasing α [23]. Hence, the maximum effective dopant fraction can be estimated by setting $\tau_\epsilon \approx \tau_a$, which results in $\alpha \approx \delta_\epsilon \nu_m / k_a n_g \approx 4\%$ for $\delta_\epsilon \approx 10 \times (2m_e/m_{H_2})$. Figure 10 shows, indeed, the equilibrium electron density can be reduced by more than two orders of magnitude with a dopant fraction of $< 1\%$. Since $Z = 70$ for SF_6 and $Z = 96$ for c-C_4F_8, too much dopant fraction will cause enhanced beam-impact ionization and multiple scattering with the dopant gas.

For most dopant gases, the probability of electron capture drops to zero for high energy electrons. For SF_6, the upper energy limit is as low as 0.4 eV, while c-C_4F_8 has finite attachment cross section at up to 1 eV (see Fig. 9).

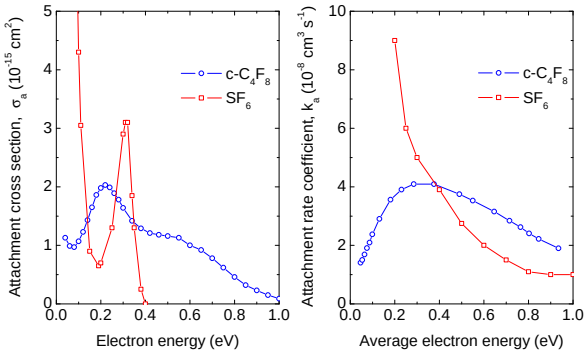

FIG. 9: Electron attachment cross section as a function of electron energy (left), and electron attachment rate coefficient as a function of average electron energy of Maxwellian distribution (right) for dopant gases, c-C_4F_8 and SF_6.

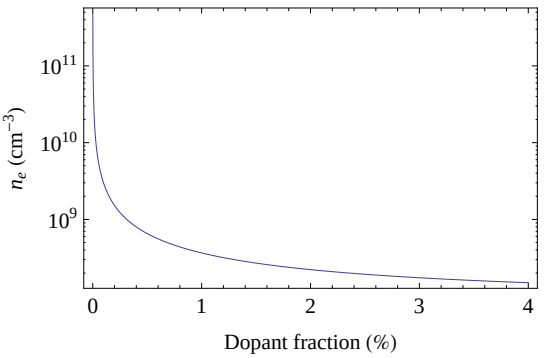

FIG. 10: Equilibrium electron density as a function of dopant fraction for $k_a \approx 2 \times 10^{-8}\mathrm{cm}^3\mathrm{s}^{-1}$ and $\delta_\epsilon \approx 10 \times (2m_e/m_{\mathrm{H}_2})$.

VI. SUMMARY AND CONCLUSION

The beam test planned for the HPRF cavity at Fermilab will be an important milestone for the future direction of ionization cooling channel development. One concern is the possible accumulation of plasma induced by beam-impact ionization. Since recombination and dissociative attachment are quite slow, the plasma is expected to be locally accumulated over the macropulse duration and absorb a considerable amount of RF power. To mitigate this effect, use of a small fraction of dopant gas has been discussed.

APPENDIX A: MOBILITY

Even though the linear relation $\nu_m \propto p$ is convenient for theoretical analysis, it is no longer accurate when $E/p < 4$ [14]. Tollestrup [5] shows that energy loss by the electron plasma can be more accurately calculated in terms of the mobility μ for high collisional regime where an electron behaves as it would in a DC electric field. The mobility relates drift velocity v_d and RF electric field $E(t) = E_0 \sin(\omega t)$ as $v_d = \mu E(t)$. Using the empirical equation obtained by Heylen [16], we can rewrite the drift velocity as

$$v_d[\mathrm{cm/s}] \approx 100 \left(\frac{2e}{m_e}\right)^{1/2} \times \tilde{\mu}\left(\frac{E}{p}\right), \qquad \text{(A1)}$$

where E/p is given in $\mathrm{Vcm}^{-1}\mathrm{torr}^{-1}$ and a parameterized function $\tilde{\mu}$ is given for $0.1 < E/p < 100$ by

$$\tilde{\mu} = 1.72{\times}10^{-2}\left[1 - 2.4 \times 10^{-2}\left(\frac{E}{p}\right)^{0.71}\right]^{-1.75}\left(\frac{E}{p}\right)^{-0.53}. \qquad \text{(A2)}$$

On the other hand, when the collision frequency for momentum transfer is approximately given as $\nu_m \approx 4.4 \times 10^9 p[\mathrm{torr}]$ [13, 14], the drift velocity becomes

$$v_d[\mathrm{cm/s}] = \frac{e}{m_e \nu_m} E \approx \frac{e}{m_e(4.4 \times 10^9)} \times \left(\frac{E}{p}\right). \qquad \text{(A3)}$$

Here, E/p is again given in $\mathrm{Vcm}^{-1}\mathrm{torr}^{-1}$. Comparison between the two drift velocity calculations is shown in Fig. 11.

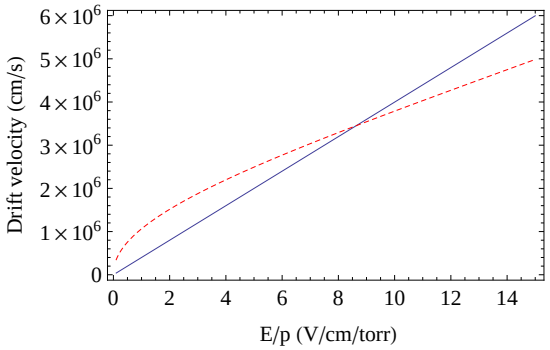

FIG. 11: Drift velocity of electrons in hydrogen molecules is plotted as a function of E/p either using Eq. (A1) (red dotted line) or Eq. (A3) (blue straight line).

The energy loss/cycle in a unit volume of the plasma is calculated as

$$P_c = \frac{n_e}{2\pi/\omega}\int_0^{2\pi/\omega} v_d(t) \times eE(t)dt, \qquad \text{(A4)}$$

which is equivalent to Eq. (16) when Eq. (A3) is used for calculating v_d. To calculate the energy loss accurately at low E/p regime while taking advantage of simple analytical description using collision frequency, we define a dimensionless parameter $\chi(E_0/p)$, which is the ratio of the energy loss calculated using Eq. (A1) to Eq. (A3). The factor χ represents the modification in energy loss calculation due to the nonlinearly in the relation between v_d and E/p. For the typical muon cooling channel parameters of $E_0 = 16$ MV/m and $p = 200$ atm ≈ 3000 psi, we have $E_0/p \sim 1$ $\mathrm{Vcm}^{-1}\mathrm{torr}^{-1}$ and $\chi \sim 3$.

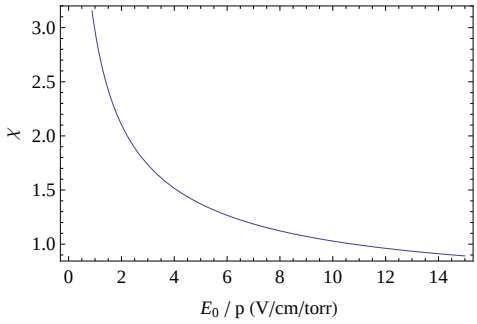

FIG. 12: Ratio of energy loss calculated using Eq. (A1) to energy loss calculated using Eq. (A3).

APPENDIX B: APPLICATION TO THE MUON COLLIDER BEAM

The final goal of the HPRF cavity experiment is to test the feasibility of using the gas-filled cavity in the actual

muon cooling system such as Helical Cooling Channel (HCC) [29]. One of the important figure of merit is the cavity degradation effect from the accumulated electrons, which scales as

$$\Delta\left(\frac{1}{Q}\right) \propto \frac{\chi N_L}{\nu_m} \propto \chi\frac{dE}{dx} \times (\text{particles per bunch}). \quad \text{(B1)}$$

Here, χ is the dimensionless parameter defined in Appendix A. Since $dE/dx \approx 4$ MeVcm^2/g for minimum ionizing muons, and $\chi \sim 3$ for typical HCC operation, we found that a single bunch with $\sim 10^9$ protons with $dE/dx \approx 10$ MeVcm^2/g and $E_0/p \sim 1$ in the HPRF is equivalent to $\sim 2.5 \times 10^9$ minimum ionizing muons. Due to the recombination process, there is no significant accumulation of beam-induced electrons after 300 micropulses (see Fig. 7). Hence, the maximum muon beam intensity that the HPRF can test is about $\sim 7.5 \times 10^{11}$ or $\sim 4.7 \times 10^{10}$/bunch for 16 bunches.

APPENDIX C: BEAM-IMPACT IONIZATION CROSS SECTION

The number of beam induced electrons can also be estimated using the ionization cross section for proton beam in hydrogen gas, which is given by [28]

$$\sigma_b[\text{cm}^2] \approx 1.3 \times 10^{-20}\beta^{-2}\left[\ln\left(1.9 \times 10^5\beta^2\gamma^2\right) - \beta^2\right]. \quad \text{(C1)}$$

The electron line density accumulated after one micropulse ($\sim 10^9$ protons) of the beam passes through the cavity is then

$$N_L = n_e\pi r_b^2 \approx \sigma_b n_{\text{H}_2} \times 10^9. \quad \text{(C2)}$$

If we compare this number with the previous calculation using the stopping power [Eq. (10)], we note that

$$\frac{\sigma_b n_{\text{H}_2}}{\rho(dE/dx)/Wi} \sim \frac{1}{2}. \quad \text{(C3)}$$

This is because the production of the secondary electron/ion pairs due to the ejected electrons is not included in Eq. (C2).

[1] D. Neuffer, Particle Accel. **14**, 75 (1983).
[2] D. Neuffer, Nucl. Instr. and Meth. A **350**, 27 (1994).
[3] D. Neuffer, Nucl. Instr. and Meth. A **532**, 26 (2004).
[4] R. P. Johnson, M. M. Alsharo'a, R. E. Hartline, M. Kuchnir, T. J. Roberts, C. M. Amkenbrandt, A. Moretti, M. Popovic, D. M. Kaplan, K. Yonehara, et al., in *Proceedings of LINAC 2004* (2004), p. 266.
[5] A. V. Tollestrup, NFMCC-doc-514-v0 (2007).
[6] W.-M. Yao, C. Amsler, D. Asner, R. Barnett, J. Beringer, P. Burchat, C. Carone, C. Caso, O. Dahl, G. D'Ambrosio, et al., Journal of Physics G **33**, 1+ (2006), URL `http://pdg.lbl.gov`.
[7] D. V. Ross, C. Thoma, D. R. Welch, and R. E. Clark, in *Low Emittance Muon Collider Workshop (Fermilab)* (2008).
[8] V. L. Highland, Nucl. Instr. and Meth. **129**, 497 (1975).
[9] M. Berger, J. Coursey, M. Zucker, and J. Chang, *ESTAR, PSTAR, and ASTAR: Computer Programs for Calculating Stopping-Power and Range Tables for Electrons, Protons, and Helium Ions (version 1.2.3). [Online] Available: http://physics.nist.gov/Star [2009, January 27]* (National Institute of Standards and Technology, 2005).
[10] I. Ben-Itzhak, V. Krishnamurthi, K. D. Carnes, H. Aliabadi, H. Knudsen, U. Mikkelsen, and B. D. Esry, J. Phys. B: At. Mol. Opt. Phys. **29**, L21 (1996).
[11] J. S. Yoon, M. Y. Song, J. M. Han, S. H. Hwang, W. S. Chang, B. J. Lee, and Y. Itikawa, J. Phys. Chem. Ref. Data **37**, 913 (2008).
[12] F. Sauli, *Principles of Operation of Multiwire Proportional and Drift Chamber* (CERN, Geneva, 1975).
[13] D. J. Rose and S. C. Brown, Phys. Rev. **98**, 310 (1955).
[14] Y. P. Raiser, *Gas Discharge Physics* (Springer-Verlag, Berlin, 1991).
[15] G. Bekefi and S. Brown, Phys. Rev. **112**, 159 (1958).
[16] A. E. D. Heylen, in *Proceedings of the Physical Society* (1960), p. 779.
[17] S. C. Brown, *Basic Data of Plasma Physics* (John Wiley and Sons, New York, 1959).
[18] Y. Xu and I. I. Fabrinkant, Appl. Phys. Lett. **78**, 2598 (2001).
[19] R. Celiberto, M. Capitelli, and A. Laricchiuta, Physica Sripta. **T96**, 32 (2002).
[20] P. G. Datskos and L. A. Pinnaduwage, Phys. Rev. A **55**, 4131 (1997).
[21] K. Nakashima, H. Takagi, and H. Nakamura, J. Chem. Phys. **86**, 726 (1987).
[22] A. Y. Pigarov, Physica Sripta. **T96**, 16 (2002).
[23] M. B. Reid, J. Appl. Phys. **73**, 4212 (1993).
[24] J. C. Slater, Rev. Modern Phys. **18**, 441 (1946).
[25] F. F. Chen, *Introduction to Plasma Physics and Controlled Fusion* (Plenum Press, New Youk and London, 1984).
[26] N. Kriby, M. Berry, I. Blumenfeld, M. J. Hogan, R. Ischebeck, and R. Siemann, in *Proceedings of PAC 07* (2007), p. 3097.
[27] R. J. Goldston, *Introduction to Plasma Physics* (Institute of Physics Publishing, Bristol and Philiadelphia, 1995).
[28] M. Reiser, *Theory and Design of Charged Particle Beams* (Wiley-VCH, Weinheim, 2008), 2nd ed.
[29] Y. Derbenev and R. P. Johnson, Phys. Rev. ST Accel. Beams **8**, 041002 (2005).